JAST
Journal of Aerospace Science and Technology

Pages: 116-128/ Vol. 15/ No. 1 /Winter- Spring 2022

Journal of Aerospace Science and Technology

www:jast.ias.ir

Scientific- Researsh Article

Numerical study on enhancement of low speed axial compressor rotor performance under radial inlet distortion via DBD plasma actuators

Ali Khoshnejad [1*], **Reza Ebrahimi**[2], **Sohrab Gholamhosein Pouryoussefi**[3]

1-2-Combustion and Propulsion Research Laboratory, Department of Aerospace Engineering, K. N. Toosi University of Technology

3- Aerodynamic Research Laboratory, Department of Aerospace Engineering, K.N.Toosi University of Technology

ABSTRACT

***Keywords**: Axial Compressor, Inlet Distortion, Plasma Actuator, Active Flow Control, Stall Margin.*

Aero-engine entrance conditions are not always ideal, and, for various reasons, inlet distortion may occur and cause inlet blockage and reduction of compressor performance. This study aimed to numerically simulate the effects of plasma actuators on the enhancement of low-speed axial compressor rotor performance under radial inlet distortion. First, compressor performance was investigated under radial inlet distortion with 15% and 20% blockage and their destructive effects on stall margin. Then, the effect of plasma actuators on rotor loss subjected to inlet distortion was investigated, using an algebraic model based on the plasma actuators' physics in the form of body force distribution in Naiver-Stokes equations. The results show that radial inlet distortion decreases the compressor's stall margin. In addition, according to the findings, applying plasma actuators boosts the flow momentum behind the distortion screen and reduces the blockage of the rotor tip region, leading to decreasing losses. Furthermore, at 15% blockage, the plasma actuators increase the stall margin from -11% to -5% versus the rotor in clean condition.

Introduction

Achieving high safety and increasing the operating range of aero-engine compressors are two critical purposes in designing aero engines. Sometimes the inlet conditions of the fan and the aero-engine compressors are not ideal, and also, in some cases, the flow separation causes to create disturbances and distortions at the engine intake, which exposes the compressor to aerodynamic instabilities. Many scientific researchers have discussed the design and development of compressors and fans in which the conditions of the inlet instabilities do not affect them. Consequently, their performance does not decrease.

The inlet distortion is defined as non-uniformity in the properties of the inlet flow to the engine [1]. This non-uniformity is known as one of the most important factors in creating instabilities, which reduces the axial velocity and increases the incidence angle of the flow to the blades of the first row of the compressor [2]. These flow distortions affect the stability range of the compressor, and

1 PhD. Candidate (Corresponding Author) **Email: *** a.khoshnejad@email.kntu.ac.ir
2 Professor
3 Assistant Professor

DOI : 10.22034/jast.2021.309899.1102
Submit: 10-10-2021 / Accepted: 09.11.2021
Print ISSN:1735-2134 Online ISSN: 2345-3648

their destructive effects cause a stall and even serge in the compressor [1]. When the compressor operates under the conditions of inlet distortion, the stalling process occurs at a higher flow coefficient, which means that the stability range of the compressor is reduced [3]. Some factors can lead to flow distortion at the inlet of the compressor and the inlet fan of the aero-engine, such as atmospheric vortices, fast maneuvers of fighter aircraft in the vortex created by other aircraft, the effect of vortices caused by weapon equipment, the bird strike to aircraft engine, strong crosswinds, compact inlets duct with high curvature [4]. Another factor that causes non-uniform flow at the inlet of new engines is the advanced and novel arrangement and shape of the inlet duct of these engines, two of which are serpentine and S-type inlets [4].

These non-uniformities and disturbances occur in the form of pressure changes, temperature changes, the creation of swirling flow [5], and density changes. However, in most cases, the flow disturbances show themselves as total pressure changes at the inlet [6]. Many researchers have investigated the destructive effect of inlet flow disturbances on compressor performance experimentally and numerically [7, 8]. Baffle-shaped distortions are the main methods of simulating inlet distortions, which are divided into two categories [9]: static distortion, which includes constant radial [10, 11] circumferential [12] or combined distortions, and dynamic distortion, such as rotating distortions [13]. In fact, radial distortions occur due to the increase in the thickness of the boundary layer at the inlet, significantly affecting the compressors' performance [14].

In an experimental study, Sundercock et al. investigated the effects of radial inlet distortions on a blade row in a transonic compressor. This study showed that radial inlet distortions at the tip of the rotor blade row reduce the compressor stall margin. Schmidt et al. also experimentally investigated the effect of radial inlet distortions at an axial fan's rotor blade row tip and hub. This investigation showed that this type of inlet distortion at the tip and hub of the rotor reduces the stage pressure ratio and the stall margin. In 2020 Jichao et al. investigated the effects of this type of inlet distortion on the aerodynamic stability of a multistage axial compressor [14]. This research used two types of inlet flow distortions at the hub and tip of the compressor rotor. Performance and unsteady measurements were done under the conditions of these types of inlet distortions in the compressor. The results of this research showed that the radial inlet distortions at the tip of the blade row of the compressor reduce the stall margin by 3.5%. In addition to experimental research, this type of inlet distortion has also been studied in various numerical research [15, 16].

The interaction of the tip leakage flow and the main flow passing through the passage between the two blades creates the tip leakage vortex. On the other hand, the tip radial inlet distortions decrease the axial velocity of the flow at the tip region. Therefore, this type of inlet distortion causes the tip leakage vortex movement towards the blade's leading edge, which leads to premature stall and high losses in the tip of the blade in the compressor [11, 17].

In recent decades, researchers have used various active and passive flow control methods to improve the stall margin and increase the operating range of compressors under the condition of inlet distortion [18]. The casing treatment method is the most used passive method in controlling the inlet disturbance to the compressor. Also, some studies have investigated the use of inlet guide vanes to improve the performance of compressors [19]. Moreover, the flow injection method at the rotor blade row of the compressor is the most well-known active method in various types of research [17]. Spakovszky et al. performed an experimental study to control the flow instabilities caused by inlet distortion by the air jet injection control method. The result of the study showed that the radial inlet distortions in a compressor with NACA 35 rotor blade row reduce the stall margin by 10%. Meanwhile, the air jet injection method improved the compressor stall margin by 17% under the condition of inlet distortion [20]. However, using the air jet injection method as an active control method requires different equipment that adds subsystems to the engine, increasing the engine's complexity and weight.

Using DBD plasma actuators as an active control method is a novel and innovative method in turbomachinery, especially in improving the performance of axial compressors. DBD plasma actuators are two or more electrodes separated by a dielectric material. In this method, the momentum of the particles in different regions is increased by the plasma discharge in such a way

that applying a high-frequency voltage between the two electrodes creates a strong electric field and locally ionizes the air molecules (producing cold plasma). Then, an induced and local momentum is added to the flow by the collision of moving charged particles with neutral air particles, which creates an induced force in the surrounding fluid field [21]. Hence, this method's advantages in flow control have made it attractive and valuable in controlling flow instabilities in turbomachines [22]. These plasma actuators have several advantages, including small size and low weight, fast response, no moving parts, small size, no adverse effect on the main flow, cheap and affordable price, and high reliability. [23]. A review of the research on using plasma actuators to modify aerodynamic characteristics shows that most flow control studies have been performed on external aerodynamics [24]. In contrast, few studies have investigated the use of plasma actuators in turbomachines. Accordingly, the effect of plasma actuators on controlling inlet disturbances in axial compressors has yet to be evaluated in the literature, and studies have only investigated the effect of these actuators in controlling tip leakage flow.

Vo et al. presented the concept of using plasma actuators in tip leakage flow control in axial compressors [25] and numerically evaluated the most optimal location of actuators in controlling tip leakage flow. This study's results show that installing plasma actuators upstream of the rotor and at a distance of 7% of the blade chord length is the most optimal place for controlling the tip leakage flow and delaying the occurrence of a stall in a low-speed compressor. In 2012, Jothiprasad et al. used a linear volumetric force distribution in numerical simulations to model plasma actuators. They evaluated the effect of this active control method in enhancing the stall margin of a low-speed axial compressor. This study showed that applying the induced force created by the plasma actuators opposite direction of the rotational speed is the most optimal configuration to delay the stall occurrence [26]. In 1400, Khoshnejad et al. numerically evaluated the effect of using plasma actuators on the physics of tip leakage vortex and investigated the losses caused by this phenomenon in a rotor blade row of the low-speed axial compressor. The results showed that plasma actuators reduce the losses caused by the tip leakage vortex and improve the stall margin of the compressor [23].

In addition to numerical studies, various experimental studies have been carried out in low-speed [27] and high-speed [28] axial compressors to investigate the effect of plasma actuators in increasing the stall margin. In an experimental-numerical study, Ashrafi et al. (2014) investigated the effect of plasma actuators on increasing the stall margin in a low-speed axial-centrifugal compressor. They used a low-speed compressor prototype with dielectric casing and blades, and the results showed that the plasma actuator improves the stall margin of axial and centrifugal compressors [27]. In another experimental study, Thomas Cork et al. (2017) investigated the application and effect of DC pulsed plasma actuators on stall control in an axial fan, in which the use of a DBD plasma actuator was tested to prevent or delay rotating stall in an axial fan. The obtained results showed that the improvement of the stall margin was up to 5% in the performance curve of the fan, which was due to the fact that by reducing the power of rotating oscillations by using the plasma actuators, the flow coefficient of the stall was decreased and consequently the stall margin of the fan was improved [29].

This numerical paper examines the effect of plasma actuators in controlling instabilities and disturbances created due to radial distortion upstream of a low-speed axial compressor rotor. Also, the flow field in the compressor is simulated under the condition of radial flow distortion with 15% and 20% of blockage, and the effects of these distortions are evaluated on the compressor performance. In the next step, plasma actuators were applied upstream of the rotor blade row of the compressor as an active control method to manage instabilities. Accordingly, the ability of this method has been evaluated in reducing the losses created due to these flow distortions. Moreover, the reduction of the undesirable effects of radial flow distortions in an axial compressor and its control have been investigated using plasma actuators. The main purpose of this study is to enhance rotor the stall margin, reduce the loss caused by flow distortions by using plasma actuators, and improve the tip leakage flow structure in different operational conditions.

Rotor geometry and flow distortion screens

In this simulation, an isolated rotor blade row is used based on the NACA-65 series, including 12 blades, and the flow passing through the rotor passage is in the subsonic range. Also, the rotational speed of the rotor is considered equal to 1300 rpm. Table 1 shows some characteristics of this geometry used in various studies [30, 31].

Table 1. Geometric characteristics of the axial compressor rotor

characteristic	unit	value
Number of blades	–	12
Rotational speed	rpm	1300
Hub radius	mm	135
Hub to tip ratio	–	0.6
The ratio of tip gap to blade chord length	%	1.7
Chord length at the tip	mm	117.5
Tip stagger angle	deg	56.2

As mentioned in the introduction, a simulation using a radial distortion screen upstream of the blade tip area was performed to study the effect of boundary layer thickness growth at the casing of axial compressors on its performance. The effect of inlet distortions has been investigated by adding radial distortion screens in the rotor inlet, which are installed with a blockage percentage of 15% and 20% of the flow inlet area at a distance of 5 times compared to the axial chord length of the blade tip (Cax) on upstream of the leading edge of the rotor. Figure 1 shows the distortion screens and their location.

Methodology and Numerical Scheme

Numerical Simulation Method

Simulations are considered for the entire rotor passages to model the effects of flow distortion. The solution domain of this simulation is divided into four blocks, including the stationary block with flow distortion, the rotor inlet block, the rotating block, and the outlet stationary block. The Ansys CFX commercial software is used to solve the Navier-Stokes equations in an incompressible and steady-state form. This software has the capability of three-dimensional analysis of the flow to solve the governing equations, including conservation of mass (Equation 1) and momentum equation (Equation 2) in rotational coordinates using the finite volume method. The turbulence model used in this study is the kω-SST, known as a proposed model in turbomachinery problems due to its high accuracy in high-pressure gradient flows and applying the modifications around the wall [23]. The residual values in the main equations are considered in the range of 10^{-7} to converge the numerical simulation.

$$\frac{\partial}{\partial t}(\rho)+\frac{\partial}{\partial x_i}(\rho u_i)=0 \quad (1)$$

$$\frac{\partial}{\partial t}(\rho u_i)+\frac{\partial}{\partial x_j}(\rho u_i u_j)=-\frac{\partial p}{\partial x_i}+\frac{\partial}{\partial x_j}(\tau_{ij}-\overline{\rho u_i' u_j'})+F_i \quad (2)$$

$$\tau_{ij}=\mu\left[\frac{\partial u_i}{\partial x_j}+\frac{\partial u_j}{\partial x_i}-\frac{2}{3}\delta_{ij}\frac{\partial u_l}{\partial x_l}\right] \quad (3)$$

$$Fi=-\rho[2\Omega\times U+\Omega\times\Omega\times r] \quad (4)$$

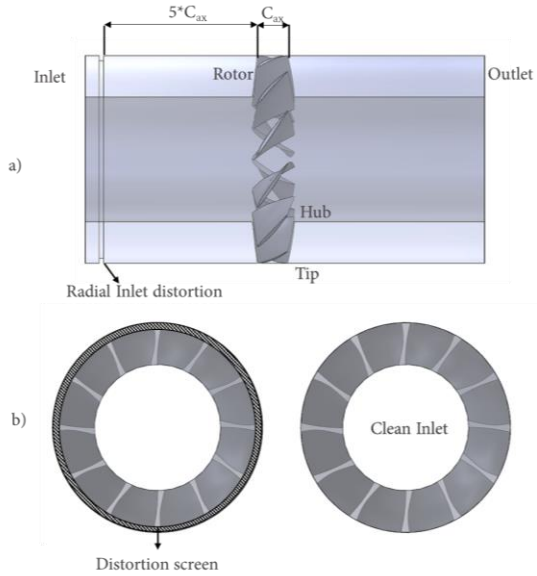

Figure 1. rotor blade row with flow distortion screen, a) side view of the computational domain with the flow distortion screen, b) front view of the blade in the condition without flow distortion and with flow distortion screen

Meshing

Turbogrid and Ansys Meshing software have been used to produce multi-block meshing of the rotor passage and area of flow distortion block, respectively. In this meshing, 777118 elements are considered for each rotor passage, including the rotor's inlet, the rotating block, and the outlet block. So that 598670 elements are related to the rotating block, 80408 elements are related to the rotor inlet block, and 98040 elements are related to the outlet block. Consequently, a total of 9325416 elements are considered for the simulation of 12 passages, and 286344 elements are considered for the block of the inlet distortion region. 30 elements

are considered radially in the 2 mm rotor tip clearance region to simulate the plasma model efficiently, and the mesh density around the wall (y+) is less than 5. Figure 2 shows the mesh distribution structure on the blade and its hub in the computational domain. Figure 3 also shows the meshing in the rotor passage.

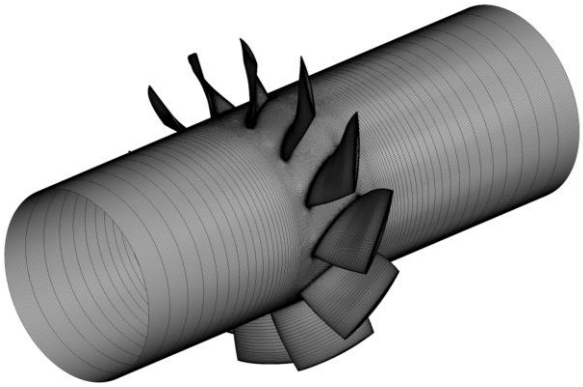

Figure 2. Meshing on the wall of the computational domain

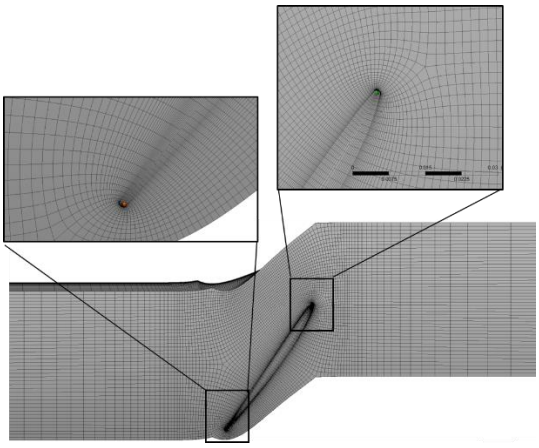

Figure 3. Meshing in the rotor passage

To ensure the meshing quality used in this simulation, the independence of the obtained results from the number of elements has been evaluated, which was done for a rotor passage and considering the variable of the total pressure rise coefficient in the passage. Figure 4 shows the results of this evaluation, which includes different types of meshing, from large to small meshes. This figure shows that the best number of meshes for this rotor passage is 777118 elements. Following that, negligible changes are observed in the pressure rise coefficient.

Model of plasma actuators

To evaluate the effect of plasma actuators on the control of the inlet disturbances of the rotor caused by radial distortions in these numerical simulations, the fluid dynamic effects of these actuators have been implemented to control these flow disturbances. Therefore, the actuators are placed at a distance of 7% of the blade tip chord length and upstream of the rotor. This distance has been suggested in various studies as the optimal value for low-speed rotors [25]. This method is effective in the injection of momentum to the low-velocity area created behind the radial distortion. It also increases the velocity of the inlet flow to the rotor, which is schematically shown in Figure 5.

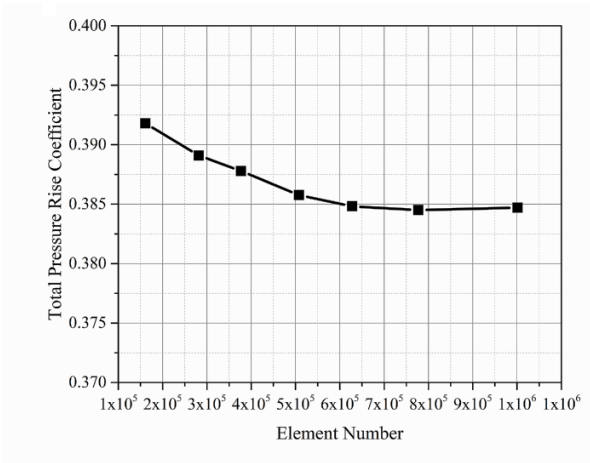

Figure 4. Grid independency results

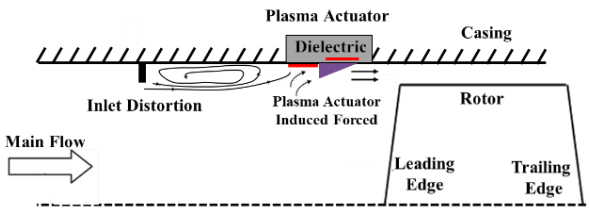

Figure 5. Schematic of the installation of plasma actuator and flow distortion screen

An algebraic model based on plasma physics, presented by Shyy [32], was used to implement the fluid dynamics effects of plasma actuators as a flow control method to inject local momentum to flow. In this method, the distribution of the induced force of plasma actuators has been presented as an algebraic model that is proportional to the dimensions of the actuators, applied voltage and frequency, and the dimensions of the electrodes. This efficient model has been used in various applications in aerodynamics in recent years [33] due to its low computational cost and appropriate accuracy. Hence, these advantages make it one of the most suitable models for identifying the effect of plasma actuators on controlling disturbances of the inlet flow to a

compressor [25]. Ansys CFX software was used to model this method, and CEL programming language was also used to implement this volumetric force distribution. Finally, this distribution was added to the Navier-Stokes equations as an additional term for generating momentum. Through the observations and experimental tests, Shyy et al. presented a model based on the linear distribution of volumetric force created due to plasma effects in a small triangular area with a length of b=3 mm and a height of a=1.5 mm. Figure 6 shows the electric field distribution of Shyy's algebraic model, according to which the smaller length and width of this area are evident compared to the diameter of the compressor.

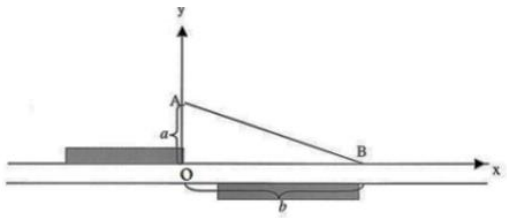

Figure 6. linear electric field intensity distribution in Shyy's model [32]

In this model, the changes in electric field intensity are linear. They are defined according to equation 5, where the variable Eo is the intensity of the electric field at the beginning of the applying area of plasma actuators and is calculated according to equation 6. In these equations, V and d are the maximum voltage between two electrodes and the distance between them, respectively.

$$|E| = E_o - k_1 x - k_2 y \tag{5}$$

$$E_o = \frac{V}{d} \tag{6}$$

The constant values k_1 and k_2 are calculated using equations 7 and 8, respectively. In the following two equations, E_{cr} is the intensity of the electric field in the breakdown state, which is calculated by considering the intensity of the electric field in the boundary between the plasma and fluid region and is equal to the breakdown value (in the direction of the A-B line). The components of the electric field in the directions of x and y are calculated using equations 9 and 10, respectively It is important to note that the electric field's intensity below the A-B line is lower than the intensity of the electric field in the breakdown state.

$$k_1 = \frac{E_o - E_{cr}}{b} \tag{7}$$

$$k_2 = \frac{E_o - E_{cr}}{a} \tag{8}$$

$$E_x = \frac{Ek_2}{\sqrt{k_1^2 + k_2^2}} \tag{9}$$

$$E_y = \frac{Ek_1}{\sqrt{k_1^2 + k_2^2}} \tag{10}$$

$$(F_x, F_y) = E\alpha\rho_c e_c f\,\Delta t\left(\frac{k_2}{\sqrt{k_2^2 + k_2^2}}, \frac{k_1}{\sqrt{k_2^2 + k_2^2}}\right) \tag{11}$$

Finally, the volumetric force distribution is calculated using equation 11, fully explained in the study [25]. Table 2 shows the variables used in this equation and their values. The duration of plasma discharge (Δt) is very small compared to the time scales in fluid flow, and this volumetric force is only applied to the fluid during the time Δt (time of plasma formation). This time is only half of the alternating flow cycle, and the plasma production is done only during this time. Therefore, the volumetric force obtained in the second half of this cycle is ignored due to the lack of plasma production or a very small amount of it. Also, due to the high discharge frequency, the force applied to the fluid is assumed to be a constant average force concerning time, which is constant throughout the cycle. In this simulation, the applied frequency and voltage are considered 3 kHz and 4 kV, respectively.

Table 2. Characteristics of the variables used in the simulation of Shyy's model [32]

Variable	symbol	unit	value
Applied frequency	f	kHz	3
Total charge density	ρ_c	1/cm^3	10^{11}
Time of plasma discharge	Δt	s	$10^{-6} * 67$
Breakdown electric field	E_b	kV/cm	30
Applied voltage	U_a	kV	4
Efficiency factor	α	-	1
The height of the plasma region	a	mm	1.5
The width of the plasma actuator region	b	mm	3
Distance between plasma actuators	d	mm	0.25
The exposed length of the electrode	–	mm	0.5
Covered electrode length	–	mm	3
Electrode height	–	mm	0.1

Results

Validation of compressor performance curve

The numerical simulation of this paper was validated in the condition without plasma actuators and flow distortion with the experimental results presented in reference [34] at a rotational speed of 1300 rpm. The results of this validation are shown in Figure 7. In this figure, the compressor performance curve obtained from numerical simulation is compared with the experimental results, which are presented in terms of the total pressure rise coefficient (ψ) before and after the rotor versus the flow coefficient (ϕ) in the rotor. The values of the total pressure rise coefficient and the flow coefficient in this diagram are calculated using equations 12 and 13, respectively. In these equations, ΔP_t, U_t, and C_x are the total pressure difference before and after the rotor, the velocity at the tip of the blade, and the axial velocity of the rotor inlet, respectively. According to this figure, the results obtained from the numerical simulation are consistent with the experimental results. Figure 8 compares the results of the total pressure rise coefficient in the radial direction of the blade with the experimental results, which shows the high accuracy of the numerical simulation.

$$\psi = \frac{\Delta P_t}{\frac{1}{2}\rho U_t^2} \tag{12}$$

$$\phi = \frac{C_x}{U_t} \tag{13}$$

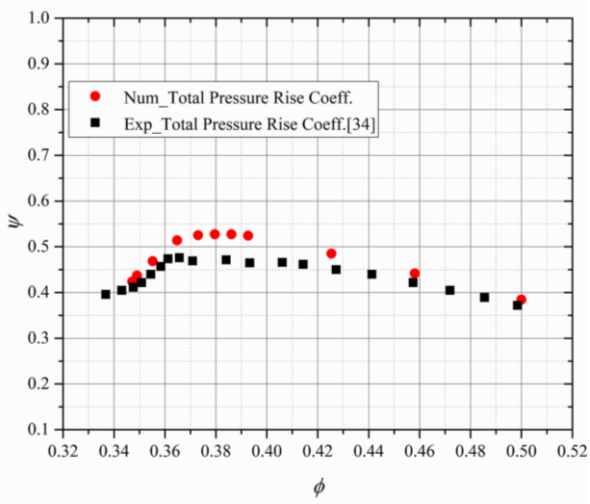

Figure 7. Validation of the compressor performance curve (1300 rpm)

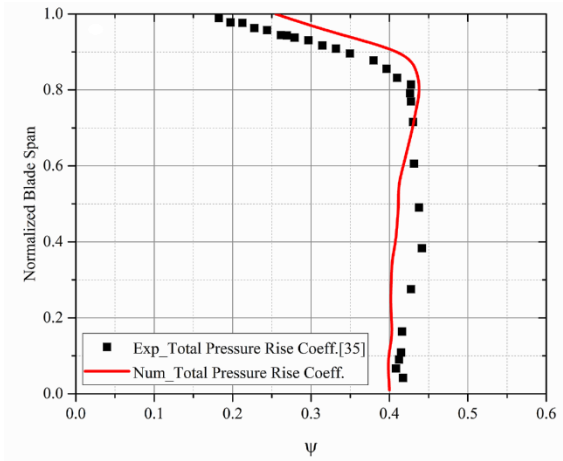

Figure 8. Validation of total pressure rise coefficient distribution along the blade span

Plasma model validation

In this simulation, the plasma actuators are placed at a distance of 7% of the chord length of the blade tip upstream of the rotor and on the casing to control the instabilities created due to the radial distortions. Moreover, the plasma model has been validated to add this model to the Navier-Stokes equations. First, this model is used on the flat plate according to the reference geometry [32], and the results are compared with the reference results shown in Figure 9. This comparison is performed at the voltage of 4 kV and the frequency of 3 kHz. The obtained results of this diagram indicate the high matching between the simulation and the reference results. After modeling validation, the plasma model was also applied to an annular cylinder casing by mapping the cartesian force distribution into cylindrical coordinates. Indeed, the plasma model is implemented on the inner surface of the cylinder, and its induction flow is simulated. Figure 10 shows the related results. The results of Shyy's model applied to the cylindrical casing show that the general effects of plasma actuators on the cylinder are similar to their effects on the flat plate.

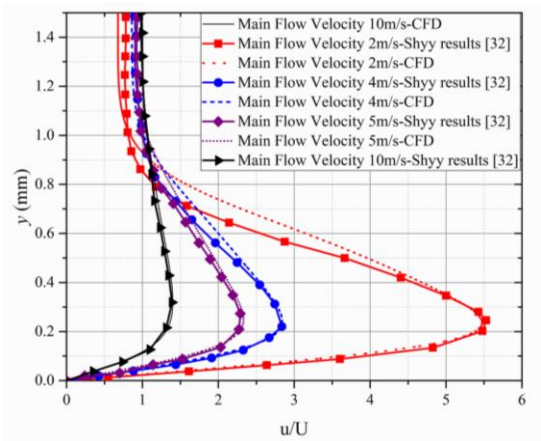

Figure 9. Results of plasma actuators applied on a flat plate at different free flow velocities and according to the geometry of Shyy's study

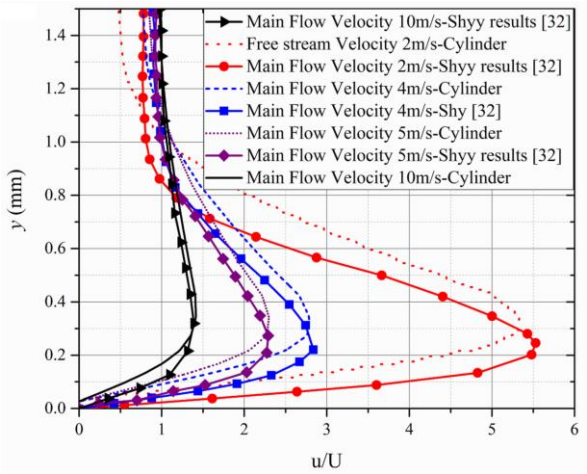

Figure 10. Results of plasma actuators applied to the cylinder at different free flow velocities

The effect of plasma actuator on flow distortion

The effect of plasma actuators has been evaluated in different operational conditions of the compressor with 15% and 20% blockage at the rotational speed of 1300 rpm, presented as the compressor performance curve in Figure 11. This figure shows that in the condition without flow distortion, plasma actuators increase the stall margin of the compressor. In other words, the total pressure rise coefficient increases in the area near the stall, and the stall flow coefficient is reduced. It is important to note that the stall is proportional to the areas where the pressure rise coefficient decreases as the flow coefficient decreases. This figure shows that flow distortion with the percentages of 15% and 20% reduces the stall margin of the compressor and causes premature stall (creating stall at higher flow coefficients), which increases by increasing the blockage percentage. The plasma actuator improves the rotor's performance in the flow distortion condition, which is more in 15% blockage. Indeed, by increasing flow distortion, the effectiveness of plasma actuators to flow control has decreased.

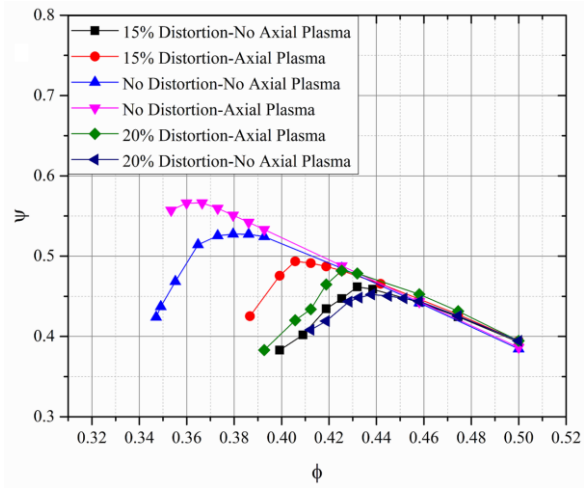

Figure 11. compressor performance curve in different operational conditions (RPM 1300)

One of the methods that can express the destructive effects caused by inlet distortions and determine the effectiveness of flow control methods in compressors is the displacement of stall points in different operational conditions. The relative changes are presented with two approaches to quantitatively examine the amount of changes in the stall margin and the pressure rise coefficient of the stall in different operational conditions. The first approach evaluates the amount of changes in different conditions compared to the base state without flow distortion and plasma actuators. On the other hand, the second approach evaluates the number of changes in the stall flow coefficient and the total pressure rise coefficient in the presence of flow distortion and plasma actuators. One of the methods presented in the literature references for investigating the number of changes in compressor stability is equation 14, which shows the relative changes in the flow coefficient compared to the two different conditions.

$$\Delta\varphi = \left[(\varphi_{stall})_1 - (\varphi_{stall})_2\right] / (\varphi_{stall})_1 \qquad (14)$$

Figure 12 shows the changes in stall margin and pressure rise coefficient in different conditions compared to the base state, without plasma actuator and inlet distortion. According to this figure, the plasma actuators increase the stall margin of the compressor by about 5 % in the

condition without inlet distortion. Also, this figure shows that the flow distortion screen with blockage percentages of 15% and 20% has caused a 12% and 17% reduction in the compressor stall margin, respectively.

Applying plasma actuators to inject momentum to the low energy area behind the flow distortion screens has partially restored the inappropriate conditions created due to the radial flow distortions, which can be seen in the total pressure rotor coefficient in the rotor. As shown in Figure 12, the flow distortion screen with a percentage of 15% reduces the total pressure rise coefficient by about 16%. Furthermore, applying the plasma actuator in the same conditions reduces the pressure rise coefficient by about 10%, which shows the effectiveness of the plasma actuator. Figure 13 shows the changes in the stall margin and the total pressure rise coefficient in the rotor under different inlet distortions with blockage of 15% and 20% with the presence of plasma actuators. As shown in this figure, applying plasma actuators in the condition with 15% blockage improves the stall margin by 6% and improves the total pressure rise coefficient in the rotor by about 7%. Also, the stall margin is increased by about 2.8% in the flow blockage by 20%, and the total pressure rise coefficient is increased by about 6.5%.

The loss coefficient of the rotor is another variable that can be used to evaluate the undesirable effects of flow distortion and the effects of plasma actuators in improving performance in the rotor. The rotor loss coefficient in reference [34] is calculated using equation 15, where C_θ is the tangential velocity and is calculated as an average from the hub to the tip of the blade. Also, the 1 and 2 indices indicate the plane before and after the rotor. The rotor loss coefficient was validated in design conditions by comparing the results of numerical simulation with the experimental results of the reference [34], shown in Figure 14. This figure shows that the simulation results are consistent with the experimental results. According to this figure, it is clear that the blade hub and tip are the main sources of loss in the flow passage. According to this figure and due to the installation of radial flow distortion in the blade tip region, the flow passage loss in the blade tip region is expected to increase.

$$\zeta_p = \frac{(u_2 c_{\theta 2} - u_1 c_{\theta 1}) - \Delta P_t / \rho}{U_t^2 / 2} \qquad (15)$$

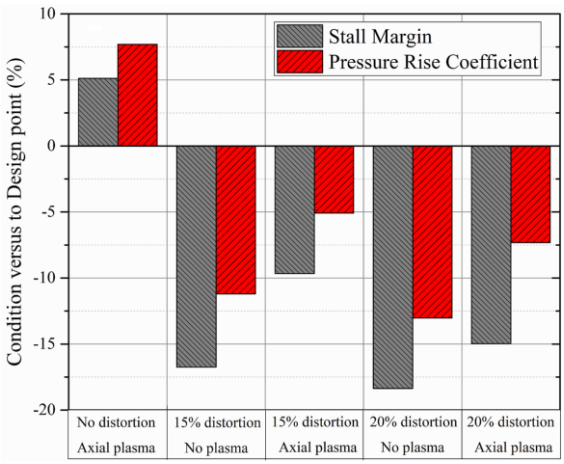

Figure 12. Changes in the stall margin and the total pressure rise coefficient in different conditions compared to the state without distortion and plasma actuator

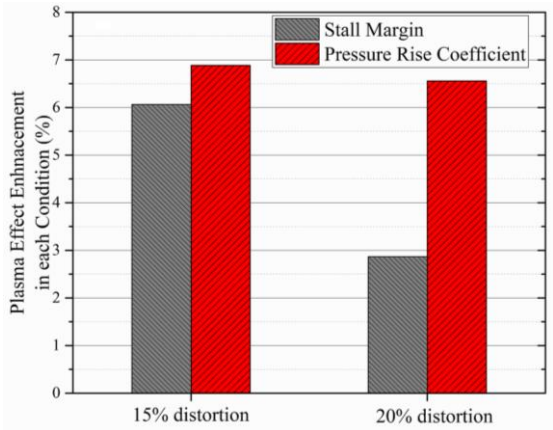

Figure 13. Changes in the stall margin and the total pressure rise coefficient of the rotor with different distortion screens with plasma actuators

Figure 15 shows the effect of radial inlet distortions with different percentages on the distribution of the loss coefficient along the blade span. Also, it shows the effect of plasma actuators with the presence of flow distortions on the rotor loss coefficient at the flow coefficient of 0.43. As is evident in this figure, the presence of a 20% radial inlet distortion screen in the blade tip area causes the most significant amount of loss in the blade tip area. Also, applying plasma actuators has reduced the loss coefficient in the presence of flow blockage. In fact, applying plasma actuators has improved the adverse effects of flow blockages.

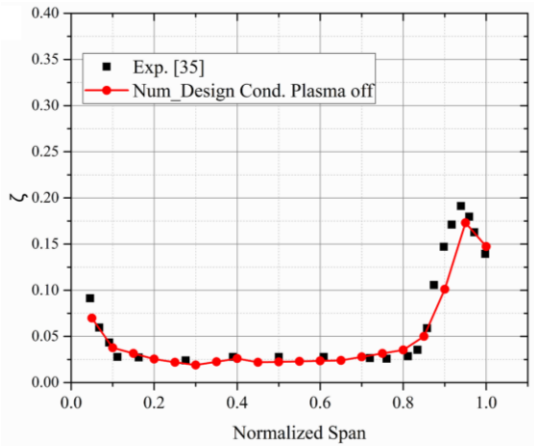

Figure 14. Validation of the loss coefficient distribution along the rotor span in design conditions

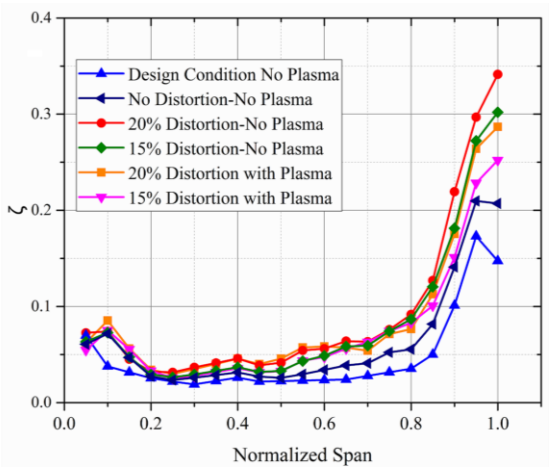

Figure 15. Distribution of a loss coefficient along the rotor span in flow coefficient of 0.43 and different operational conditions

As mentioned before, radial inlet distortions of the blade increase the flow loss at the tip, which causes premature stall and reduces the stall margin. However, plasma actuators reduce the undesired effects of these instabilities by injecting momentum in the tip leakage region.

Figure 16 shows the effect of plasma actuators on reducing the loss in the rotor tip leakage area in the dimensionless relative total pressure contour, which is in the front view and at a distance of x/Ca=0.15 (x is axial distance from the leading edge of the rotor) and in the operational conditions at the flow coefficient of 0.43 in the presence of flow distortion screen with the percentage of 15% and 20%, with and without applying the plasma actuator. It should be noted that the values of this diagram have become dimensionless compared to the dynamic pressure of the blade tip flow in the design conditions. In Figure 16, dark areas show the region with high losses. In this figure, it is clear that by increasing the percentage of flow distortion, the amount of losses in the blade tip area increased. However, applying the plasma actuators decreases this loss due to the injection momentum in the low energy area of the tip leakage region. Also, the comparison of figures 16-a and 16-c shows that by applying plasma actuators, the area with high loss gets close to the blade's suction surface and reduces the losses and distortion in this area of the passage. Figure 17 shows the dimensionless axial velocity contour in the rotor passage at 0.97% of the blade span and the flow coefficient of 0.43 in different operational conditions. In this figure, the axial velocity values become dimensionless compared to the linear velocity of the blade tip in the design condition at the flow coefficient of 0.5. With the presence of a flow distortion screen, negative velocity increases, representing the reverse flow in the rotor passage. This issue is more severe in the flow distortion of 20% than in the flow distortion of 15%. Also, the comparison of Figure 17-a with Figure 17-b shows that in the flow distortion with blockage of 15%, applying the plasma actuators cause to transfer area with low velocity into the rotor passage, which reduces the flow distortion in this area. While in flow distortion of 20%, the amount of passage distortion areas is more than the flow distortion of 15%. Therefore, plasma actuators improve the flow field. Also, it can be seen in this figure that by increasing the amount of flow distortion, the effectiveness of plasma actuators also decreases.

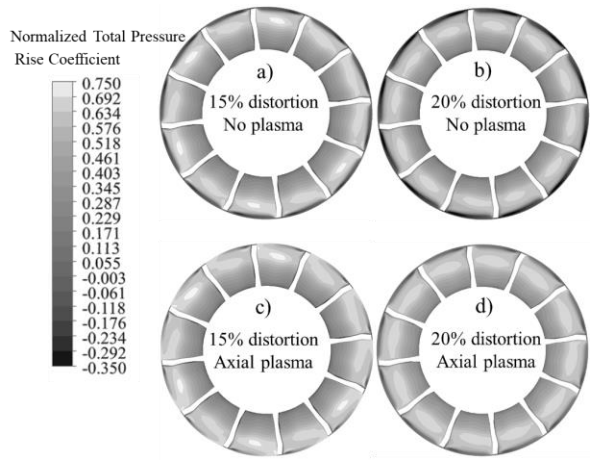

Figure 16. total pressure contour in relative coordinates, from the front view of the compressor section and in the middle part of the blade in operational conditions at a flow coefficient of 0.43 and at an axial distance of x/Ca=0.15 from the leading edge of the rotor

Conclusion

This paper investigates the effect of plasma actuators in controlling disturbances created due to radial distortions upstream of an isolated blade row of a low-speed axial compressor. First, the flow field in the compressor is simulated in the condition with radial inlet distortions of 15% and 20%. Then, the destructive effects of this type of disturbance on the overall performance of the compressor are evaluated. Next, by using plasma actuators as a novel active control method, the ability of these actuators to recover the undesired conditions created due to disturbances in the compressor is evaluated. Accordingly, the most important results obtained from this research are as follows:

1) Radial inlet distortion affects the compressor rotor's overall performance, which reduces compressor performance, increases losses in the blade tip leakage region, and causes a premature stall in the compressor.
2) By increasing the percentage of radial inlet distortion from 15% to 20%, the stall margin of the compressor decreases from -11% to -13%. In general, the performance of the rotor decreases with the increase in distortion percentage.
3) Plasma actuators improve the performance of the rotor in the condition of radial distortions by injecting the momentum into the low-velocity area behind the flow distortion screens.
4) At a flow distortion of 15%, the plasma actuators increase the stall margin from -11% to -5%, indicating a positive effect of this active control method to reduce the undesired effects of flow distortion.
5) By increasing the flow distortion percentage, the plasma actuator's effect decreases. Also, these actuators only affect the tip leakage region and do not affect the main flow field between the rotor passage.

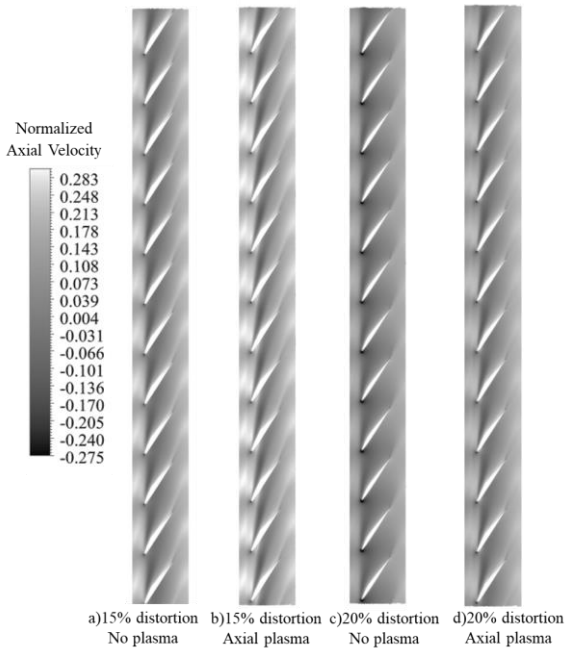

Figure 17. Dimensionless axial velocity contour at 0.97 blade span, for different operational conditions at flow coefficient of 0.43

References

[1] C. Stevens, E. Spong, and M. Hammock, "F-15 inlet/engine test techniques and distortion methodologies studies. Volume 1: Technical discussion," 1978.

[2] C. Tan, I. Day, S. Morris, and A. Wadia, "Spike-type compressor stall inception, detection, and control," *Annual review of fluid mechanics*, Vol. 42, pp. 275-300, 2010.

[3] M. Zhang and A. Hou, "Investigation on stall inception of axial compressor under inlet rotating distortion," *Proceedings of the Institution of Mechanical Engineers, Part C: Journal of Mechanical Engineering Science*, Vol. 231, pp. 1859-1870, 2017.

[4] J. F. Ryman, "Prediction of Inlet Distortion Transfer Through the Blade Rows in a Transonic Axial Compressor," Virginia Tech, 2003.

[5] Y. Zhou, J. Li, and G. Song, "Experimental investigation and detached-eddy simulation of compressor aerodynamic performance in inlet distortion," *AIP Advances*, Vol. 9, p. 065202, 2019.

[6] A. Mehdi, "Effect of swirl distortion on gas turbine operability," 2014.

[7] K. Lee, B. Lee, S. Kang, S. Yang, and D. Lee, "Inlet distortion test with gas turbine engine in the altitude engine test facility," *AIAA Paper*, vol. 4337, p. 2010, 2010.

[8] C. Mistry and A. Pradeep, "Experimental investigation of a high aspect ratio, low speed contra-rotating fan stage with complex inflow distortion," *Propulsion and Power Research*, vol. 3, pp. 68-81, 2014.

[9] F. Li, J. Li, X. Dong, D. Sun, and X. Sun, "Influence of SPS casing treatment on axial flow compressor subjected to radial pressure distortion," *Chinese Journal of Aeronautics*, vol. 30, pp. 685-697, 2017.

[10] M. A. Bennington, J. D. Cameron, S. C. Morris, C. Legault, S. T. Barrows, J.-P. Chen, *et al.*, "Investigation of tip-flow based stall criteria using rotor casing visualization," in *Turbo Expo: Power for Land, Sea ,and Air*, 2008, pp. 641-651.

[11] A. Naseri, M. Boroomand, and S. Sammak, "Numerical investigation of effect of inlet swirl and total-pressure distortion on performance and stability of an axial transonic compressor," *Journal of Thermal Science*, vol. 25 ,pp. 501-510, 2016.

[12] H. Lu, Z. Yang, T. Pan, and Q. Li, "Non-uniform stator loss reduction design strategy in a transonic axial-flow compressor stage under inflow distortion," *Aerospace Science and Technology*, vol. 92, pp. 347-362, 2019.

[13] X. Dong ,D. Sun, F. Li, D. Jin, X. Gui, and X. Sun, "Effects of rotating inlet distortion on compressor stability with stall precursor-suppressed casing treatment," *Journal of Fluids Engineering*, vol. 137, 2015.

[14] J. Li, J. Du, Y. Liu, H. Zhang, and C. Nie, "Effect of inlet radial distortion on aerodynamic stability in a multi-stage axial flow compressor," *Aerospace Science and Technology*, vol. 105, p. 105886, 2020.

[15] N. Charalambous, T. Ghisu, G. Iurisci, V. Pachidis, and P. Pilidis, "Axial compressor response to inlet flow distortions by a CFD analysis," in *Turbo Expo: Power for Land, Sea, and Air*, 2004, pp. 1637-1649.

[16] R. V. Chima, *A three-dimensional unsteady CFD model of compressor stability* vol. 4241, 2006.

[17] J. Li, J. Du, S. Geng, F. Li, and H .Zhang, "Tip air injection to extend stall margin of multi-stage axial flow compressor with inlet radial distortion," *Aerospace Science and Technology*, vol. 96, p. 105554, 2020.

[18] X. Dong, D. Sun, F. Li, and X. Sun, "Stall margin enhancement of a novel casing treatment subjected to circumferential pressure distortion," *Aerospace Science and Technology*, vol. 73, pp. 239-255, 2018.

[19] A. Maddi, R. Mohammadi Shaharaki and A. Mesgarpour Toosi, "Investigation of the effect of the inlet guide vane on the performance of the multi-stage compressor using 3D simulation," Journal of Aerospace Sciences and Engineering, Volume 13, Number 2, pp. 77-84, 2019.

[20] Z. Spakovszky, H. Weigl, J. Paduano, C. Van Schalkwyk, K. Suder, and M. Bright, "Rotating stall control in a high-speed stage with inlet distortion: Part I—radial distortion," *Journal of Turbomachinery*, vol. 121, pp. 510-516, 1999.

[21] R. McGowen, T. C. Corke, E. H. Matlis, R. Kaszeta, and C. Gold, "Pulsed-DC plasma actuator characteristics and application in compressor stall control," in *54th AIAA Aerospace Sciences Meeting*, 2016 ,p. 0394

[22] D. E. Ashpis and D. R. Thurman, "Dielectric Barrier Discharge (DBD) Plasma Actuators for Flow Control in Turbine Engines: Simulation of Flight Conditions in the Laboratory by Density Matching," *International Journal of Turbo & Jet-Engines* ,vol. 36, pp. 157-173, 2019.

[23] A. Khoshnejad, R. Ebrahimi, G. Pouryoussefi, and A. R. Doostmahmoudi, "Numerical Simulation of Plasma Actuator Effect on Control of Tip Leakage Vortex in Low Speed Axial Compressor Rotor," *Journal of Mechanical Engineering*, 2020.

[24] M. P. Patel, T. T. Ng, S. Vasudevan, T. C. Corke, and C. He, "Plasma actuators for hingeless aerodynamic control of an unmanned air vehicle," *Journal of Aircraft*, vol. 44, pp. 1264-1274, 2007.

[25] H. D. Vo, "Suppression of short length-scale rotating stall inception with glow discharge actuation," in ASME Turbo Expo 2007: Power for Land, Sea, and Air, 2007, pp. 267-278.

[26] G. Jothiprasad, R. C. Murray, K. Essenhigh, G. A. Bennett, S. Saddoughi, A. Wadia, et al., "Control of tip-clearance flow in a low speed axial compressor rotor with plasma actuation," 2012.

[27] F. Ashrafi, M. Michaud, and H. Duc Vo, "Delay of rotating stall in compressors using plasma actuators," Journal of Turbomachinery, vol. 138, p. 091009, 2016.

[28] S. Saddoughi, G .Bennett, M. Boespflug, S. Puterbaugh, and A. Wadia, "Experimental investigation of tip clearance flow in a transonic compressor with and without plasma actuators," Journal of Turbomachinery, vol. 137, p. 041008, 2015.

[29] R. C. McGowan, T. C. Corke, E .H. Matlis, R. W. Kaszeta, and C. X. Gold, "Pulsed-DC plasma actuation for stall control in an axial fan," in 2018 AIAA Aerospace Sciences Meeting, 2018, p. 1357.

[30] R. Taghavi Zenouz, M. Ababaf Behbahani, F. Rousta, and A. Khoshnejad, "Experimental investigation on flow unsteadiness during spike stall suppression process in an axial compressor via air injection," *Proceedings of the Institution of Mechanical Engineers, Part G: Journal of Aerospace Engineering*, vol. 231, pp. 2677-2688, 2017.

[31] R. T. Zenouz, M. H. A. Behbahani, and A. Khoshnejad, "Experimental investigation of air injection effects on rotating stall alleviation in an axial compressor," *Modares Mechanical Engineering*, vol. 16, pp. 267-274, 2016.

[32] W. Shyy, B. Jayaraman, and A. Andersson, "Modeling of glow discharge-induced fluid dynamics," *Journal of applied physics*, vol. 92, pp. 6434-6443, 2002.

[33] M. G. De Giorgi, V. Motta, and A. Suma, "Influence of actuation parameters of multi-DBD plasma actuators on the static and dynamic behaviour of an airfoil in unsteady flow," *Aerospace Science and Technology*, vol. 96, p. 105587, 2020.

[34] M. Inoue, M. Kuroumaru, and M. Fukuhara, "Behavior of tip leakage flow behind an axial compressor rotor," 1986.